International Journal for Housing Science and Its Applications

Publish September 9, 2025. Volume 47, Issue 1 Pages 629-641

https://doi.org/10.70517/ijhsa47154

Unsupervised Deep Curve Estimation Network with Automated Parameter Adjustment for Low-Light Agriculture Image Enhancement

Jun Li[1,2], Changqing Ye[1,2], Miao Yu[1], Yanmeng Chen[1], Chenping Zeng[1,2,*], Chaoyun Yang[1], Wenfeng Wang[1] and Hui Zhu[1]

[1] School of Information Technology, Xichang University, Xichang, Sichuan, 615013, China

[2] Key Laboratory of Liangshan Agriculture Digital Transformation of Sichuan Provincial Education Department, Xichang, Sichuan, 615013, China

Corresponding authors: (e-mail: zengchenping@xcc.edu.cn).

Abstract Images of agricultural products—such as tobacco leaves, tea leaves, Chinese medicinal herbs, edible fungi, and dehydrated vegetables—captured in enclosed environments often suffer from poor illumination, color distortion, and significant background noise. These challenges impede accurate monitoring of color changes and reliable quality assessment. Existing low-light enhancement methods in smart agriculture are constrained by their reliance on large, high-quality annotated datasets. To address this, we propose DynZero-DCE, a rule-based dynamic zero-reference deep curve estimation framework tailored for agricultural low-light imaging. The method introduces: (i) a rule-based dynamic adjustment that adapts enhancement to per-image statistics, (ii) a cubic curve with piecewise luminance control for exposure stabilization, (iii) cross-scale local feature fusion and an edge-preserving denoising residual that suppresses noise amplification while maintaining leaf venation details. Trained without paired references, our losses enforce exposure consistency, color fidelity, and structural preservation. On a curated dataset, DynZero-DCE improves clarity by up to 32.9× and brightness by up to 15.7×. These results demonstrate superior luminance balancing, color faithfulness, and detail rendering under extreme low-light conditions.

Index Terms low-light image enhancement, zero-reference, rule-based dynamic adjustment, edge-preserving denoising, agricultural imaging, tobacco curing barns

I. Introduction

Post-harvest agricultural products—including tobacco leaves, tea leaves, medicinal herbs, fungi, and dried fruits—undergo controlled dehydration processes in enclosed environments. Precise regulation of temperature, humidity, and air circulation, coupled with energy-efficient technologies, ensures optimal product transformation. This study examines tobacco leaf flue-curing, a process comprising four sequential phases: yellowing, color fixation, stem desiccation, and lamina dehydration [1]. These procedures, which involve strategic harvesting, moisture reduction, and aroma stabilization, are critical for maintaining consistent raw material quality during processing, storage, and cigarette manufacturing.

Traditional tobacco curing is accomplished by controlling and adjusting the temperature and humidity of the curing barn. This method relies on precise environmental regulation to guide the curing process. However, such manual control approaches are labor-intensive, highly subjective, and inconsistent, struggling to meet the modern tobacco industry's requirements for precision and standardized production. In contrast, modern tobacco curers prioritize observing the color changes of tobacco leaves through barn windows to assess curing progress. These color shifts reflect transformations in the leaves' internal chemical components and serve as a core quality control indicator. With next-generation information technology, such as artificial intelligence (AI), the Internet of Things (IoT), and edge computing, the use of computer vision, IoT, and AI in tobacco production has emerged. By installing cameras in sealed curing barns to monitor changes in the color of tobacco leaves in real time, the process aims to improve efficiency. However, limited camera placement, poor lighting conditions inside the tobacco barn, underexposed images, color distortion, and noise interference hinder the accurate recognition and quantification of the leaves' key color characteristics. These challenges significantly limit the effectiveness of computer vision in curing tobacco leaves. Curing barns present: (i) severe underexposure and highly nonuniform illumination from localized heating elements; (ii) color cast from lamp spectra; (iii) specular highlights on waxy leaf surfaces causing local saturation; (iv) smoke-like veiling, reducing local contrast; and (v) occasional motion blur from

ventilation/handling. Collecting paired references is infeasible; thus, a zero-reference deep curve estimation (DCE) approach enables pixel-wise exposure control without paired ground truth. In our design, exposure consistency (Lexp), color fidelity (Lcolor), spatial/structure preservation (Lspa and Sal), and coefficient-space denoising are aligned to these barn-specific degradations.

To overcome the difficult imaging problems in tobacco-curing conditions, low-light image augmentation is essential. People frequently use three main techniques: deep learning-based, Retinex-based, and histogram-based techniques. Although histogram-based techniques, including global and adaptive histogram equalization, are effective and easy to use, they can sometimes cause photos to appear overly bright, lose important features, and increase noise, especially in complex lighting or color situations. For instance, Wang et al. [2] used adaptive block histogram equalization to better keep local details, but this led to more noise in dark and noisy images; Guan et al. [3] combined gamma correction, noise reduction, and bilateral filtering to improve contrast in infrared images. By separating images into light and color components, retinex-based techniques increase brightness and detail; however, they are computationally intensive and may result in difficulties such as color changes or halos. Wei et al. [4] developed a deep Retinex network that maintains color accuracy, while Liu et al. [5] employed a Retinex-based algorithm to restore lost features and correct uneven illumination. However, both approaches are computationally costly and rely on the quality of the data. Through sophisticated feature extraction, deep learning approaches greatly enhance image quality; nevertheless, they are prone to overfitting in complicated settings because of their high labeled data and computing requirements. In order to address these issues, Koohestani et al. [6] developed a self-calibrated illumination (SCI) system that enhances image quality and color accuracy without the need for labeled data by utilizing multi-stage learning and weight sharing. Guo et al. [7] developed Zero-DCE, which employs a model that predicts a zero-reference curve, negating the need for matching data and showcasing its versatility. While Chen et al. [8] employed transformers and attention techniques to better comprehend the whole scene and restore image details in dim lighting, Liu et al. [9] developed a versatile improvement system for industrial contexts to minimize noise.

Current low-light image enhancement techniques for tobacco leaves face notable practical limitations. CLIP [10] improves semantic understanding but lacks sensitivity to subtle color and structural differences, often introducing artifacts. CoLIE [11] utilizes contextual information for denoising but is limited in enhancing surface texture and non-uniform illumination. DRBN [12] enhances brightness but amplifies noise, degrading image quality. FLOL [13] favors speed over the precise restoration of texture and color. RUAS [14] improves generalization but remains susceptible to color casts and artifacts. ALEN [15] adapts to varying lighting but struggles to maintain texture, color accuracy, and fine details. ZeroDCE++ [16] simplifies training with unsupervised curve adjustment, yet often results in color distortion and loss of detail in complex lighting. While GAN-based methods such as CLIP provide general enhancement, they struggle with subtle color distinctions in tobacco leaves. Similarly, unsupervised curve estimation methods like ZeroDCE++ avoid the need for paired data but often produce color inaccuracies under the challenging lighting conditions found in curing barns.

To address these limitations, we propose a novel low-light enhancement framework: the Rule-based Dynamic Zero-Reference Curve Network for Low-Light Agricultural Imaging with Edge-Preserving Denoising (DynZero-DCE) Enhancement Network. By integrating color constancy principles with an efficient, lightweight architecture, our method accurately captures fine color transitions during the tobacco curing process. It requires minimal computational resources and specifically optimizes spatial contrast, saturation, and detail preservation—effectively overcoming the challenges faced by existing algorithms in extreme low-light environments.

II. Materials and Methods

Addressing the challenges of image enhancement under extreme lighting conditions in enclosed tobacco barns, this work presents an unsupervised learning-based image enhancement algorithm tailored for extreme lighting conditions encountered in enclosed tobacco barns. A comprehensive multi-luminance image dataset was developed to facilitate the training of an adaptive non-linear feature mapping network, capable of capturing the intrinsic features of such challenging environments. The proposed algorithm integrates a pixel-level constraint optimization mechanism that addresses the shortcomings of traditional methods in scenarios characterized by severe over-exposure and under-exposure. Leveraging deep learning techniques, the model learns local luminance variations and fine texture details within tobacco leaf images subjected to harsh illumination, thereby generating a precise pixel-wise mapping. Experimental results demonstrate that the proposed method substantially enhances detail preservation and overall visual quality, highlighting its potential for robust application in agro-industrial imaging systems.

Figure 1 shows the construction of the DynZero-DCE enhancement network, which generates the best ultra-low-light enhancement (ELLE) curves for photos of tobacco leaves. We apply these ELLE curves to the RGB channels of the input image for better results. In the following sections, we cover each module in the DynZero-DCE network in detail, including the construction of ELLE curves. In an unsupervised learning environment, the proposed framework enhances loss functions, minimizes noise, and improves leaf details. To address the challenges of processing images of tobacco leaves at low light levels during curing, the framework is divided into three specialized components, A, B, and C, as shown in Figure 1a. In

Segment A, the curve from ZeroDCE++ [16] is changed into a cubic function to better manage brightness, emphasize the main and secondary leaf veins, and keep important details without over-brightening or smoothing the image. Using a special method based on Equation (1), Segment B modifies pixel values in a certain way to improve images. Depending on the brightness of different areas, this technique helps to modify the image's contrast and details by strengthening darker areas and decreasing lighter ones. Through the selective amplification of low-intensity regions and the attenuation of high-intensity regions, this technique adjusts visual contrast and detail according to luminance parameters. At each level, the intensity of correction is controlled by enhancement parameters (r1 to r8) to enable precise, layer-by-layer optimization. The recursive nonlinear structure allows us to clearly model complex pixel interactions while simplifying the process of enhancing local details and brightness range while preserving important aspects. Photos that have inconsistent lighting or low contrast are good candidates for this method. Segment C combines adaptive local augmentation with edge-preserving denoising. After evaluating local contrast, the algorithm creates a luminance map and uses mean convolution to smooth it. By employing adaptive thresholding to divide the image into bright and dark regions, exposure and contrast adjustments specific to each area are made possible. In downstream procedures like leaf recognition, segmentation, and visual analysis, this content-adaptive approach reduces noise while preserving crucial information, resulting in higher-quality photos.

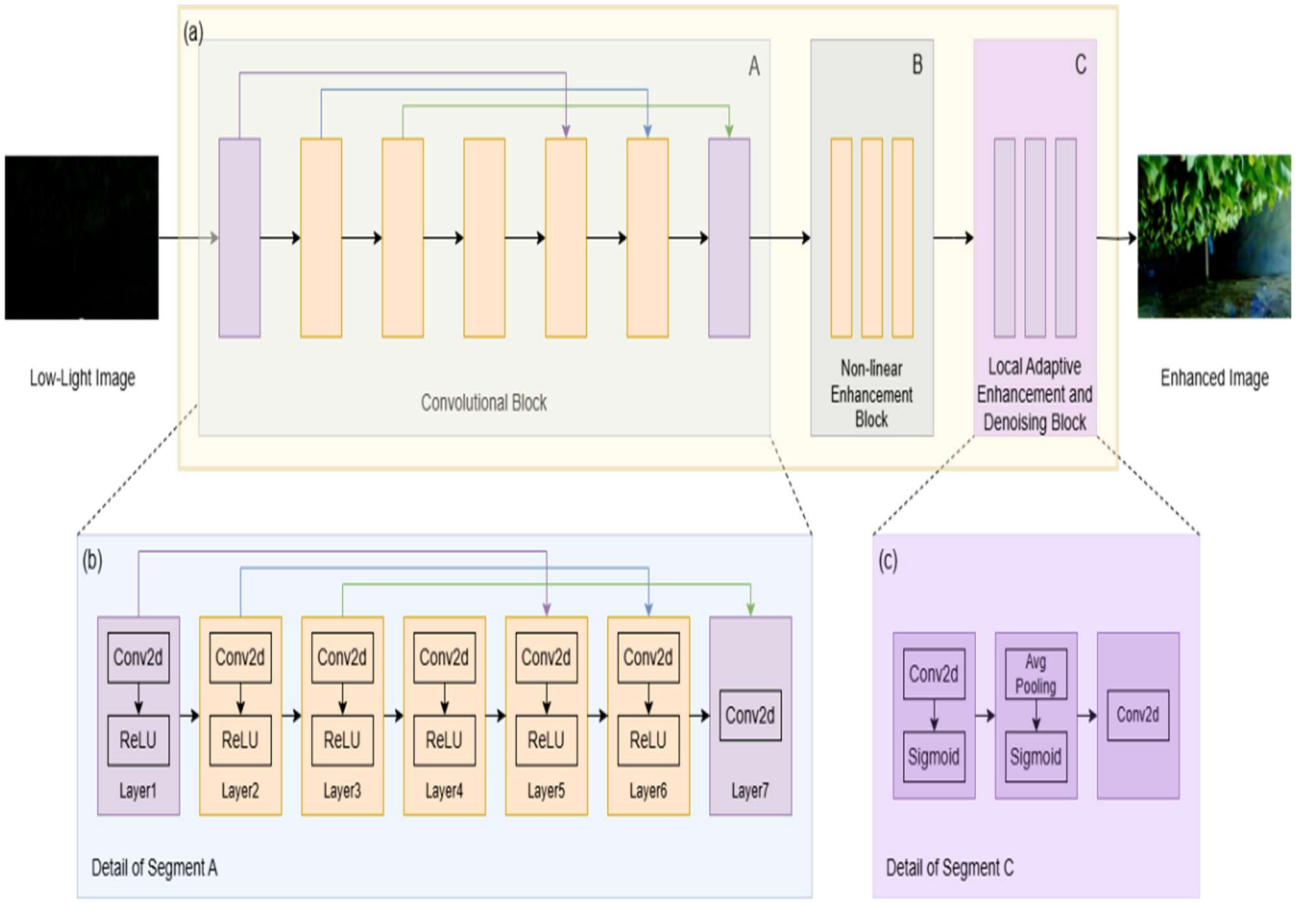

Figure 1: Network framework for low-light image enhancement. (a) The framework of the proposed rule-based dynamic adjustment zero-reference deep curve estimation (DynZero-DCE) enhancement network, which can be divided into three categories: a convolutional block, a non-linear enhancement block, and a local adaptive enhancement and denoising block; (b) the framework of the texture extraction and fusion block; and (c) the framework of the local adaptive enhancement and denoising block.

II. A. Extreme Low-Light Enhancement Curves

We tailor the curve to these degradations by using a cubic form with piecewise luminance control to stabilize exposure and preserve venation detail under nonuniform, cast-prone lighting. The Zero-DCE algorithm [15] is a general-purpose method for enhancing low-light images without a reference image. Therefore, we adapted this method to the specific imaging conditions of tobacco curing barns. A single low-light image of tobacco leaves captured in the curing barn rule-based

dynamic adjustment of a scene-adaptive enhancement curve. To better handle the complex lighting and texture characteristics of tobacco leaves during curing, we extended the original quadratic enhancement curve to a cubic form.

This modification improves the brightness of dark regions, reduces local overexposure, and enhances the visibility of the fine structures of the primary and secondary veins. Different from other general-purpose methods, our approach accounts for the unique color transitions and textural variations of tobacco leaves during curing. These include regional differences in the apex, venation, and lamina, as well as the presence of intricate textures and color gradients. To enhance structural details, We operate on normalized intensities $I(x,y) \in [0,1]$. Parameter $r \in [0,1]$. The term $I(x,y)-I(x,y)^3$ emphasizes mid-tones, aiding vein visibility while limiting saturation growth. The equation is as follows:

$$ELLE(x,y) = I(x,y) + r \cdot (I(x,y) - I(x,y)^3) \tag{1}$$

where I(x,y) represents the pixel intensity at the spatial coordinates x (horizontal) and y (vertical) within the image. The transformation is modulated by the parameter $r \in [0,1]$, while the nonlinear mapping is characterized by the expression $I(x,y)-I(x,y)^3$.

II. B. DynZero-DCE Network

Combining the deep curve estimation network [15] with the natural characteristics of tobacco leaves, we developed the new system DynZero-DCE. Compared to DCE-Net's seven-layer architecture, DynZero-DCE features a redesigned connectivity framework comprising seven hierarchical layers, with substructures A, B, and C (Figure 1) collectively constituting the complete architecture.

As shown in Fig. 1(b), DynZero-DCE enhances cross-scale feature integration by fusing the first and fourth, second and fifth, and third and sixth layers. In Fig. 1(c), combining convolution, average pooling, and Sigmoid activation improves the visibility of main and lateral tobacco veins. A contrast adjustment module, utilizing local statistics, further enables adaptive contrast enhancement while preserving fine textures, as described in Equation (2). The seventh layer output undergoes nonlinear transformation and Gaussian kernel convolution for smoothing and detail enhancement. Finally, we clamp the network output to [0,1] and convert to 8-bit [0,255] only for saving/display (PyTorch 2.1.0, CUDA 12.8).

$$E_{contrast}(x,y) = \omega_{con\_2} \cdot \left(\omega_{con\_1} \cdot ELLE(x,y) - \mu_{local}\right) + \mu_{local} \tag{2}$$

where $E_{contrast}(x)$ is the function for augmentation of image contrast, ELLE(x,y) denotes the image post-enhancement at the sixth layer, ω_{con_1} and ω_{con_2} represent two adjustment parameters, respectively, and μ_{local} represents the local mean intensity of the image.

We adopt a rule-based dynamic adjustment (see Equation (3)) using luminance quantiles of the Y channel to set thresholds for dark and bright regions. Specifically, qd and qb denote the lower and upper quantiles (defaults $q_d \approx 0.20$, $q_b \approx 0.80$, computed per image). This quantile-based design stabilizes enhancement under abrupt illumination changes. A sensitivity analysis shows low sensitivity for $q_d \in [0.15,0.25]$ and $q_b \in [0.75,0.85]$. Region-specific gains ω_{dark_1} and ω_{bri_1} are then derived from local statistics to prevent over-/under-enhancement. Conversely, the dark threshold targets shadowed areas to enhance texture and improve image depth. These parameters can be adaptively tuned according to the leaf's position on the plant (upper, middle, or lower) to account for luminance variability, thereby ensuring optimal enhancement performance.

$$E_{adapt}(x,y) = \begin{cases} \omega_{dark\_1} \cdot E_{contrast}(x,y), & E_{contrast}(x,y) \in (0,0.2) \\ E_{contrast}(x,y), & E_{contrast}(x,y) \in [0.2,0.8] \\ \omega_{bri\_1} \cdot E_{contrast}(x,y), & E_{contrast}(x,y) \in (0.8,1.0) \end{cases} \tag{3}$$

where ω_{bri_1} and ω_{dark_1} denote parameters for bright and dark regions, respectively, $E_{adapt}(x,y)$ modulates luminance and contrast. Edge-preserving denoising in Equation (4) is realized by a bilateral-filter–based residual:

$$E_{epf}(x,y) = \omega_e(x,y) \cdot E_{adapt}(x,y) + (1 - \omega_e(x,y)) \cdot E_{adapt}(x,y) \tag{4}$$

where $E_{epf}(x,y)$ represents the result of the edge-preserving denoising of the image; λ is a scalar (default 0.5), and $\omega_e(x,y)$ represents the edge weight parameter.

Algorithm 1 integrates this denoising step into the overall rule-based enhancement pipeline.

Algorithm 1: Rule-based Dynamic Adjustment (Inference)

Input: RGB image IRGB normalized to [0,1]

1) Luminance Y = 0.299R + 0.587G + 0.114B; estimate quantiles q_d, q_b.
2) Compute μ_{color}, σ_{color} over a $w \times w$ window.
3) Apply cubic curve (Eq. (1)) → ELLE.
4) Contrast adjust (Eq. (2)) using ω_{dark_1} and ω_{bri_1} from μlocal, σlocal.
5) Piecewise control (Eq. (3)) with thresholds qd, qb and gains ωdark_1, ωbri_1 from local stats.
6) Edge-preserving residual denoising (revised Eq. (4)) with ωe from gradient magnitude and σlocal.
7) Clamp to [0,1], convert to 8-bit for display if needed.

II. C. Non-Reference Loss Function

To achieve zero-reference learning in DynZero-DCE, we present a set of no-reference loss functions that can be adjusted. We design four functions—namely, color loss, spatial loss, exposure loss, and variation loss—to evaluate the quality of the enhanced images.

Color loss (L_{color}). The color loss function, as defined in Equation (5), captures the constancy of and slight changes in the appearance of color by determining the average and spread of the R(red), G(green), B(blue) channels:

$$L_{color} = \sqrt{\left(D_{pq}^2\right)^2 + \varepsilon, \left\{(p,q) | (p,q) \in \left\{(r,g),(r,b),(g,b)\right\}\right\}} \tag{5}$$

where D_{pq}, the indices p and q correspond to pairs of channels: red and green, red and blue, or green and blue, and ε is the numerical stability parameter:

$$D_{pq} = \left(\frac{E_{epf\_p}(x,y)}{max\left\{E_{epf}(x,y)\right\}} - \frac{E_{epf\_q}(x,y)}{max\left\{E_{epf}(x,y)\right\}} \right)^2 \left\{(p,q) | (p,q) \in \left\{(r,g),(r,b),(g,b)\right\}\right\} \tag{6}$$

where $E_{epf}(x,y)$ denotes the mean values of the image across the R, G, and B channels, and $\max\{E_{epf}(x,y)\}$ represents the maximum value among the R, G, and B channels.

Spatial loss (L_{spa}). The spatial loss function, as described in Equation (7), uses the Sobel gradient [17] operator to identify edges, textures, and details in images, helping to measure geometric features. Through the use of horizontal and vertical Sobel filters on both the improved and original images, this function creates gradient maps that highlight changes in intensity in different directions. The mean absolute difference between these maps serves as an accurate metric for structural similarity, with heightened sensitivity to intricate details such as the veins and textures of tobacco leaves. This method makes sure that the improved images retain important spatial features while making them easier to see, which helps to maintain the key shape characteristics that are important for assessing quality.

$$L_{spa} = \sum_{dir_i=1}^{4} D_{dir_i} + 0.5 \cdot D_{sobel} = \sum_{dir_i=1}^{4} \left(D_{org\_dir_i} - D_{enhance\_dir_i} \right)^2 + 0.5 D_{sobel} \tag{7}$$

where D_{dir} quantifies the cumulative directional differences across four orientations: left, right, up, and down. The subscript $i \in \{1,2,3,4\}$ in D_{dir} explicitly denotes these respective directions. Correspondingly, $D_{org\_dir\_i}$ and $D_{enhance\_dir\_i}$ represent the sampled values from the original and enhanced images along the identical directional axes indexed by i, while D_{sobel} signifies the differential derived from the Sobel gradient [7].

Exposure loss (L_{exp}). The exposure loss function, as defined in Equation (8), adjusts the brightness of images and improves the detail of images under different lighting conditions *through balancing local and overall brightness:*

$$L_{exp} = \frac{1}{N} \sum_{i=1}^{N} \omega_i \cdot \left(\mu_i - target_i \right)^2 \tag{8}$$

where ω_i denotes the weight coefficient for the ith sample (defined as $e^{-|\mu-0.5|}$), μ_i signifies the predicted outcome for the ith sample, and $target_i$ represents the target outcome for the ith sample, as detailed in Equation (9).

Ensuring uniformity across data sets is pivotal for enhancing numerical stability and optimizing model performance in tasks such as image classification and object detection. The target value of the ith sample signifies the actual output, label, or ground truth associated with the ith data point within a data set. This element is integral to supervised learning tasks, serving as the standard for evaluating model predictions. Through juxtaposing the predicted values with the target values, the model iteratively refines its parameters during training to minimize errors, thereby augmenting its accuracy in tasks such as classification, regression, and so on.

$$target_i = \begin{cases} 0.2, & \mu_i \in (0, 0.2) \\ \mu_i, & \mu_i \in [0.2, 0.8] \\ 0.8, & \mu_i \in (0.8, 1) \end{cases} \tag{9}$$

where μ_i represents the input value.

Variation loss (L_{TV}). The variation loss function, as defined in Equation (10), helps to prevent images from becoming too smooth, retains important texture details, and maintains the overall structure of images through examining differences in the gradients (both horizontally and vertically):

$$L_{TV} = \frac{2 \cdot TV_{Loss\_weight} \cdot \left(\frac{\sum_{x=1}^{H} \sum_{y=1}^{W} h(x,y) \left[\left(v(x,y+1) - v(x,y) \right)^2 \right]}{count_h} + \frac{\sum_{i=1}^{H} \sum_{j=1}^{W} \omega(x,y) \left[\left(v(x,y+1) - v(x,y) \right)^2 \right]}{count_w} \right)}{batch_{size}} \tag{10}$$

Herein, TV_{Loss_weight} denote the total variation loss weighting coefficient; N and M represent pixel counts along horizontal and vertical axes; B indicates the batch size; h(x,y) characterizes the height weight parameter at coordinate (i,j); v(x,y) signifies the pixel intensity; H and W define image dimensions; and ω(x,y) represents the spatial weight.

Structure-aware loss (S_{al}). The structure-aware loss, as demonstrated in Eq. (11), helps the network better understand and keep important details in images during enhancement, which helps maintain original features and minimizes the loss of textures and edges.

$$S_{a\_Loss} = \frac{1}{N} \Sigma \sqrt{\omega_r D_r^2 + \omega_g D_g^2 + \omega_b D_b^2 + \varepsilon} \tag{11}$$

where w_r, w_g , w_b represent the weights for the red, green, and blue, as seen in Eq. (13) channels, D_r, D_g, and D_b denote the deviations for the red, green, and blue channels, as seen in Eq. (12).

$$Dc = c - \mu c, c \in \{r, g, b\} \tag{12}$$

where μ_c indicates the mean value of channel c.

$$\omega_r = \frac{1}{N} \Sigma |D_r| \tag{13}$$

Total loss (L_{total}). The total loss in Equation (11) allows for a versatile assessment that takes into account the four elements defined above: overall changes, color accuracy, brightness, and spatial details:

$$L_{total} = L_{color} + L_{spa} + L_{exp} + L_{TV} + S_{al} \tag{14}$$

These four loss functions synergistically interact to quantify and optimize image quality across multiple dimensions, including chromaticity, spatial configuration, luminance, and structural integrity. Specifically, the color loss function utilizes RGB channel data to preserve color fidelity, while the spatial loss function employs the Sobel operator to detect textures and edges, thus enhancing spatial detail. The exposure loss function ensures consistent brightness under varying lighting conditions, thereby improving the visibility of fine details. The variation loss function inhibits over-smoothing, thereby maintaining the texture and structural fidelity of the image. Collectively, these loss functions facilitate detailed reconstruction and enhancement, resulting in more nuanced, expressive, and high-quality image representations.

III. Experimental Results and Analysis

In this section, we initially delineate the implementation details. Subsequently, qualitative and quantitative analyses were conducted to evaluate the performance of the proposed model in comparison with established low-light enhancement techniques. The experimental evaluation employed a dataset comprising ultra-low-light images acquired from curing barns under conditions of negligible or absent illumination.

III. A. Implementation Details

In this study, we meticulously designed experiments to qualitatively and quantitatively evaluate the efficacy of our enhancement algorithm. We benchmarked our algorithm against several cutting-edge methodologies, including CLIP [10],

CoLIE [11], DRBN [12], FLOL [13], RUAS [14], ALEN [15], ZeroDCE++ [16]. To maintain equitable conditions in the comparative analysis, all implementations were executed in Python 3.9.2, and the experiments were conducted on a Windows 10 PC equipped with 32 GB RAM, a 2.3 GHz CPU, and an NVIDIA GeForce RTX 3050 Ti Laptop GPU. To optimize low-light image enhancement, the algorithm uses the following key parameters: r in Equation (1); ω_{con_1} and ω_{con_2} in Equation (2); ω_{dark_1} and ω_{bri_1} in Equation (3); and ω_e in Equation (4).

III. B. Performance Evaluation

To ascertain the efficacy of the proposed methodology, we utilized images of tobacco leaf specimens employed in practical tobacco curing processes. The test images, derived from tobacco leaves, were subjected to a comprehensive quality assessment of the enhanced outputs. This evaluation encompassed qualitative analysis emphasizing image clarity and detail, alongside quantitative metrics including peak signal-to-noise ratio (PSNR), mean absolute error (MAE) , enhancement index (EI) , mean naturalness score (MNS) , perception-based contrast quality index (PCQI) , average gradient (AG) shannon entropy (SH), and average contrast gain (ACG).

III. B. 1) Image Enhancement Results of DynZero-DCE

Six images representing five tobacco leaf scenarios—no faint glow, faint glow, faint glow on the ground, specular reflections, and locally intense highlights—were evaluated. Qualitative results are shown in Figure 1, and quantitative results in Table 1. Each row in Figure 1 corresponds to the respective row in Table 1, excluding the header. Figure 1 shows a qualitative comparison of representative images before and after enhancement, organized as follows: rows 1–2 show images without faint glow, row 3 shows images with faint glow, row 4 shows images with faint glow on the ground, row 5 shows images with specular reflections, and row 6 shows images with pronounced local highlights. Table 1 summarizes the quantitative results, presenting statistical metrics and improvement rates before and after DynZero-DCE processing.

Table 1: The enhancement ratios of brightness and clarity were quantitatively assessed by comparing the original and processed images of six cured tobacco leaves.

Image File	Original Image Clarity [17]	Enhanced Image Clarity	Clarity Improvement Ratio	Original Image Brightness	Enhanced Image Brightness	Brightness Improvement Ratio
faint glow on the ground	118.711	232.492	1.958	24.507	114.630	4.677
without faint glow	72.233	183.680	2.543	2.450	38.691	15.792
with faint glow	6.151	202.362	32.898	3.491	53.843	15.424
specular reflections	9.917	252.288	25.439	10.979	143.788	13.097
locally intense highlights	55.976	205.640	3.674	17.634	81.781	4.638
without faint glow	7.434	225.320	30.311	5.431	80.384	14.801

The visual results and measurable improvements in image sharpness and clarity are shown in the six test images that were captured under ultra-low-light. The first and second columns of Figure 2 show the original low-light images and their histograms, which indicate that the images are too dark and unclear, with clarity scores mostly below 10 and brightness levels under 20, as presented in Table 1. In contrast, the third and fourth columns show the images after being improved by our algorithm, along with their updated histograms, which show significantly better brightness and contrast. Table 1 further quantifies these enhancements, showing that the processed images achieved clarity scores exceeding 140 and brightness levels surpassing 30. Notably, clarity improvements reached up to 32.9 times (exceeding three-fold enhancement), while

brightness improvements reached up to 15.7 times (also more than three-fold enhancement). Additionally, the second and fourth columns of Figure 2 shows how the pixel values are spread out and how often they occur, with the bottom axis showing the pixel values, the side axis showing how often they appear, and the different colors of the bars representing different pixel values. The red, blue, and green lines delineate the respective color channels, providing a detailed visualization of the algorithm's impact on each image's color composition.

III. B. 2) Comparison of DynZero-DCE's Performance with Existing Algorithms

Considering the color accuracy and detail preservation, we performed a thorough investigation focused on restoring images of tobacco leaves. Figure 3 shows visual representations of three low-light conditions: the first and second columns, respectively, display photos of tobacco leaves taken without light and their histograms; the third and fourth columns, respectively, display photos taken under reflected light and their histograms; and the fifth and sixth columns display photos taken under intense local illumination and their histograms. Eight methods were systematically evaluated to compare their performance. The proposed algorithm demonstrated effective correction of brightness anomalies, optimized luminance levels, and successfully restored the color and texture details of tobacco leaves, resulting in a well-balanced histogram. The performance of our algorithm was thoroughly evaluated under three distinct application scenarios: localized intense light, reflected light, and no direct illumination, versus seven typical techniques: CLIP, CoLIE, DRBN, FLOL, RUAS, ALEN, and ZeroDCE++. We were able to ascertain through this testing whether our algorithm is suitable for enhancing photos of tobacco leaves. As seen in Figure 3, the original images had maximum pixel values of 642,660, 313,674, and 391,880 for the three scenarios. The overall results were still visually dark and distorted in terms of color, even though CLIP increased the maximum pixel value in scenarios 1 and 2 to 698,729 and 197,975, respectively, across the comparing approaches. Even though CoLIE's highest pixel value in scenario 1 was 639,164, it still showed histogram imbalance and color distortion in high-intensity regions. In scenario 1, DRBN produced a reddish color cast, local over-enhancement, and a maximum pixel value of 100,834. In scenario 3, FLOL reached a maximum pixel value of 81,186, but it still showed a notable yellow tint. In example 1, RUAS achieved a maximum pixel value of 905,613, despite the fact that the improved images exhibited color distortion and were primarily dark. Despite having a decent pixel distribution and a maximum pixel value of 98,177 in scenario 3, ALEN suffered from local color distortion and detail loss. In scenario 2, the bulk of the histogram was in the low-value zone, and ZeroDCE++ reached a maximum pixel value of 297,988. With maximum pixel values of 173,151, 118,872, and 151,553 in the three cases, our method outperformed the others in terms of regulating brightness, balancing the R/G/B histogram, and reducing intense local light. These images demonstrate how well our method recovers balanced color and detail under challenging lighting conditions.

The proposed DynZero-DCE algorithm and the seven baseline algorithms are quantitatively compared in Table 2, with an emphasis on eight evaluation metrics: mean absolute error (MAE), average gradient (AG), Shannon entropy (SH), enhancement index (EI), perception-based contrast quality index (PCQI), naturalness image quality evaluator (NIQE), mean absolute error (MAE), average contrast gain (ACG), and peak signal-to-noise ratio (PSNR). In comparison to ALEN, CLIP, DRBN, FLOL, RUAS, ZeroDCE++, and CoLIE, the PSNR score in the second row (22.26) of Table 2 is noticeably higher, indicating how effectively our method maintains the quality and resemblance of the original images. The SSIM score of 0.51 in the third row, which is higher than all previous techniques, demonstrates how effectively the enhanced images preserve their original contrast, brightness, and structure, improving overall quality. With a score of 0.42 in the fourth row, the PCQI is the highest of all the techniques examined, suggesting improved local and global restoration of structure, color, and contrast. The fifth row, with a maximum score of 47.86, shows more obvious hierarchical layering, detailed representation, and superior information richness throughout. The AG in the sixth row, which exhibits more defined textures and structures along with enhanced edge and detail clarity, again achieves the highest rating with a score of 32.85. Out of all the strategies, the seventh row has the highest SH score (7.05), indicating enhanced sharpness, fine detail restoration, and reduced image blur. With an MNS grade of 20.91, the eighth row exhibits the highest degree of visual naturalness and conformity to how people see daylight in the real world. The ACG value of 7.83 in the ninth row, which is again the highest, significantly improves the visual hierarchy and picture contrast. Taking everything into account, these findings demonstrate that DynZero-DCE greatly enhances image quality, contrast, and naturalness, which makes it an excellent option for boosting low-light photographs.

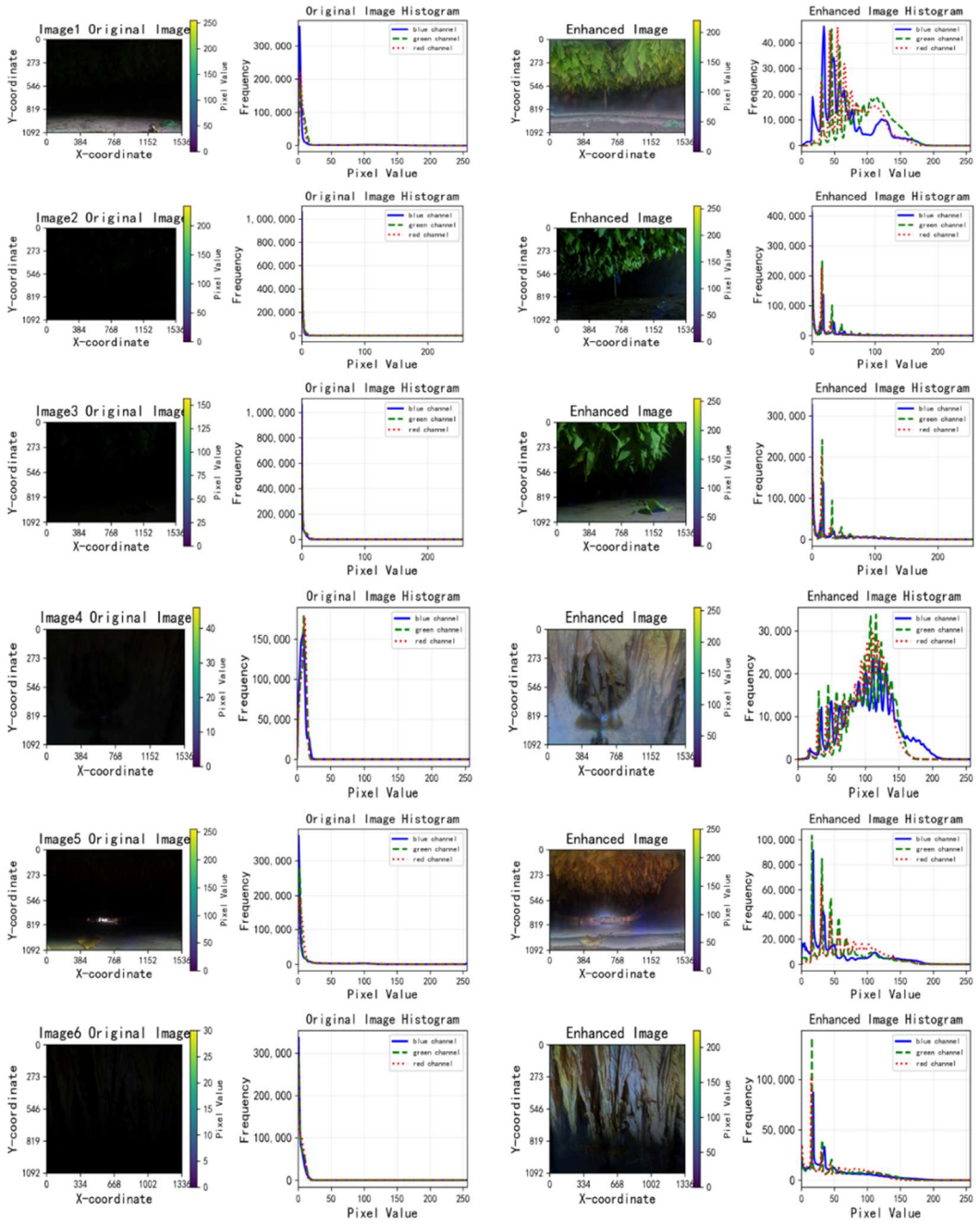

Figure 2: Examples of low-light image enhancement techniques and histogram visualization of image instances under low-light conditions: Column (a) displays the original low-light images; column (b) depicts the histograms corresponding to the original low-light images; column (c) showcases the enhanced low-light images; and column (d) presents the histograms of the enhanced low-light images.

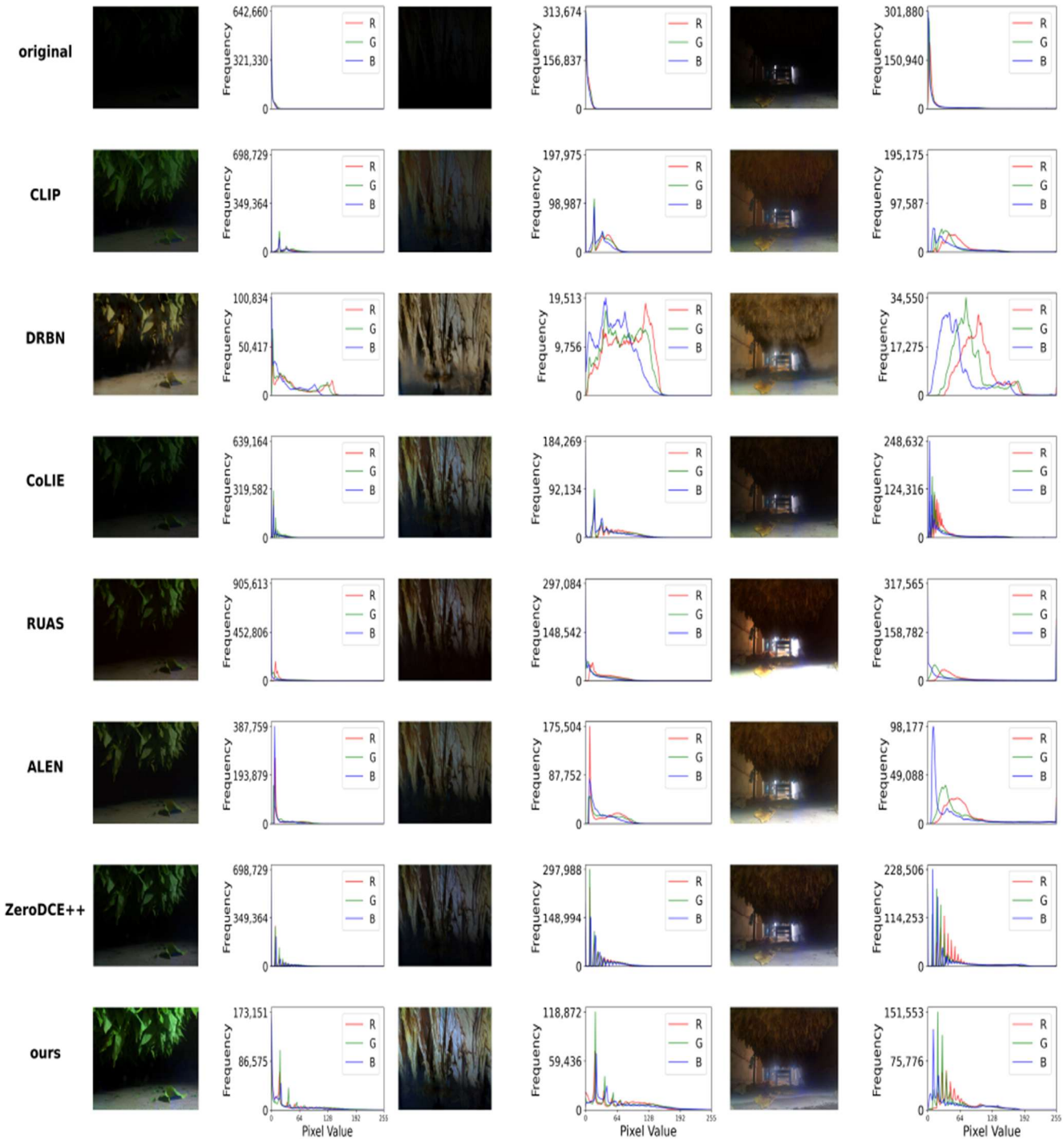

Figure 3: The efficacy of the proposed algorithm was rigorously evaluated against state-of-the-art low-light enhancement methodologies through empirical analysis on completely dark low-light images. From the top to the bottom row, the figure presents the original images, followed by the enhancement results obtained using CLIP [10], CoLIE [11], DRBN [12], FLOL [13], RUAS [14], ALEN [15], ZeroDCE++ [16], and the proposed DynZero-DCE algorithm. From left to right, the columns present the original images acquired under normal, reflected, and low-light conditions (top), respectively, each accompanied by images enhanced using different algorithms and their corresponding histograms.

Table 2: Performance comparison of eight algorithms in terms of peak signal-to-noise ratio (PSNR), SSIM (Structural Similarity Index Measure), perception-based contrast quality index (PCQI), enhancement index (EI), average gradient (AG), shannon entropy (SH), mean naturalness score (MNS), and average contrast gain (ACG). Bold values highlight the optimal result for each metric.

Method	CLIP	CoLIE	DRBN	FLOL	RUAS	ALEN	ZeroDCE++	ours
PSNR	18.25	21.68	10.89	10.70	16.55	17.10	17.68	22.26
SSIM	0.22	0.45	0.16	0.10	0.30	0.28	0.29	0.51
PCQI	0.26	0.39	0.12	0.10	0.16	0.23	0.22	0.42
EI	23.31	25.77	34.55	46.60	43.27	33.47	30.98	47.86
AG	30.13	18.53	13.61	17.18	12.09	14.57	22.66	32.85
SH	5.81	5.62	6.78	6.75	5.65	5.92	6.09	7.05
MNS	15.38	12.06	13.66	16.10	16.28	13.26	14.93	20.91
ACG	3.61	3.96	7.64	7.52	4.68	4.77	4.46	7.83

IV. Discussion

The proposed DynZero-DCE algorithm exhibits substantial improvements in processing images captured under low-light conditions. The efficiency of our algorithm across five distinct scenarios involving tobacco leaf imagery, including standard lighting, reflected lighting, dim lighting, ground-level dim lighting, and localized intense lighting, was demonstrated. These conditions present challenges such as underexposure, limited pixel differentiation, and image blurriness. The proposed algorithm mitigates overexposure, augments color fidelity, enriches informational content, and generates images with enhanced sharpness, superior contrast, and improved local detail resolution. It eliminates halo artifacts induced by weak highlights and recovers details and textures in shadowed areas, culminating in images with balanced luminance, authentic colors, clear details, esthetically pleasing visual effects, and well-distributed brightness. As shown in Figure 3, for tobacco leaf images taken under extremely low-light conditions—marked by overall darkness, low pixel variation, and unclear content—our method significantly increases information entropy compared to the seven baseline algorithms. This improvement yields sharper images, greater contrast, and enhanced local detail, effectively restoring textures in dark regions. The algorithm adaptively adjusts illumination, preserves both main and lateral vein details, reduces overexposed areas, and accurately recovers true leaf color, resulting in brighter, more natural images. Quantitative results further demonstrate the superiority of our method, with PSNR, SSIM, PCQI, EI, AG, SH, MNS, and ACG values of 22.26, 0.51, 0.42, 47.86, 32.85, 7.05, 20.91, and 7.83, respectively—each surpassing all comparative algorithms. These results highlight improved structural fidelity, brightness, and contrast, with enhanced similarity to high-quality natural images. The enhanced outputs show sharper edges, more distinct textures, reduced blur, and remarkably improved detail restoration, while better visual naturalness aligns with human perception of natural daylight scenes, particularly in contrast and hierarchical structure.

Nevertheless, the algorithm still has potential for further enhancement. It could be further improved in terms of background enhancement for low-light images; when there are weak highlights, the restored images can be too bright or display unwanted effects, making it hard to see certain areas clearly and sometimes making the bright areas look even

brighter, with some images showing random bright spots. Additionally, our algorithm does not work well in some complex or special low-light environments. Challenges such as variation in lighting, noise, and detail restoration under different scenarios still necessitate further optimization. In future work, we plan to ienhance the algorithm's adaptability and robustness under varying low-light conditions, thereby expanding its applicability to critical tasks such as nighttime pest detection, automated agricultural robot inspection, and nocturnal fruit harvesting.

V. Conclusions

This paper presents DynZero-DCE, an unsupervised deep learning framework for low-light image enhancement. The framework trains a seven-layer neural network on unlabeled low-light tobacco leaf images, enabling efficient feature learning and robust performance without manual annotation. Adaptive parameter adjustment based on regional luminance allows the framework to modulate enhancement intensity according to local lighting, effectively preventing over-enhancement and detail loss. To address the rich texture features of tobacco leaves, DynZero-DCE integrates a selective texture enhancement module, highlighting key details such as primary and secondary veins. Multi-layer feature fusion further improves the restoration of brightness and structure, delivering more natural and detailed results. Compared to existing low-light image enhancement algorithms, DynZero-DCE achieves superior performance across diverse conditions. In practical applications, especially in tobacco leaf curing and agricultural processing, the method enhances image clarity and usefulness, supporting tasks like quality inspection, pest identification, and automated sorting. Experimental results show that DynZero-DCE consistently outperforms current methods in both qualitative and quantitative evaluations, including PSNR and SSIM. Future work will focus on improving real-time processing and integrating context-aware mechanisms, Retinex theory, and unsupervised curve fitting to further enhance color restoration and detail preservation. These developments aim to extend the framework's applicability across broader agricultural and industrial computer vision tasks.

Data Sharing Agreement

The datasets used and/or analyzed during the current study are available from the corresponding author on reasonable request.

Competing Interests

The authors have no relevant financial or non-financial interests to disclose.

Acknowledgment

This article was supported by Science and Technology Planning Project of Sichuan Province,China (Grant nos. 2024YFHZ0139, and 2023YFN0094) and the Doctoral Research Start-up Project of Xichang College (Grant no. YBZ202209, and YBZ202106). The authors declare no conflicts of interest.

References

[1] Chen Z. X.; Zhang F. S.; Guo W. M.; Zang Z. Y.; Jiang S. W. IoT (internet of things)-based acquisition and analysis algorithms for temperature and humidity data during tobacco flue-curing. Tobacco Science & Technology. 2023

[2] Wang, Y.; Chen, Q.; Zhang, B. Image enhancement based on equal area dualistic sub-image histogram equalization method. IEEE Trans. Consum. Electron. 2021, 67, 230–239.

[3] Ning, K. Q.;, Gao, H. N.; Song W.; Xing N.; Li, G. Y. 2025. Histogram Equalization Algorithm Based on Guided Stratification Infrared Image Enhancement Algorithm. In Proceedings of the 2024 International Conference on Image Processing, Multimedia Technology and Maching Learning (IPMML '24). Association for Computing Machinery, New York, NY, USA, 81–87..

[4] Wei, C., Wang, W., Yang, W., & Liu, J. Deep Retinex Decomposition for Low-Light Enhancement[J]. 2018.

[5] Liu, S.; Long, W.; He, L.; Li, Y.; Ding, W. Retinex-Based Fast Algorithm for Low-Light Image Enhancement. Entropy 2021, 23, 746.

[6] Koohestani, F.; Karimi, N.; Samavi, S. Revealing Shadows: Low-Light Image Enhancement Using Self-Calibrated Illumination. In Proceedings of the 2024 32nd International Conference on Electrical Engineering (ICEE), Tehran, Iran, 14–16 May 2024; pp. 1–7.

[7] Guo, C.; Li, C.; Guo, J.; Loy, C.C.; Hou, J.; Kwong, S.; Cong, R. Zero-reference deep curve estimation for low-light image enhancement. In Proceedings of the IEEE/CVF Conference on Computer Vision and Pattern Recognition, Online, 13–19 June 2020; pp. 1780–1789.

[8] Chen, H.; Teng, Y.; Bai, Y.; Zhang. J.; Wang, J.; Li, H.; Yan, S. Learning to see in the dark with transformer. IEEE Trans. Pattern Anal. Mach. Intell. 2022, 44, 8563–8577.

[9] Liu, J.; Wang, D.; Li, H.; Zhang, J.; Guo, X.; Xu, Y.; Li, X.; Wang, J.; Li, H.; Yaan, S. Self-supervised learning-based adaptive contrast enhancement for low-light images. IEEE Trans. Image Process. 2023, 32, 1420–1435.

[10] Liang, Z. X.; Li, C. Y.; Zhou, S. C.; Feng, R. C. Loy, C. C. Iterative prompt learning for unsupervised backlit image enhancement. Proceedings of the IEEE/CVF International Conference on Computer Vision, 2023.

[11] Chobola, Tomáš and Liu, Yu and Zhang, Hanyi and Schnabel, Julia A. and Peng, Tingying. Fast Context-Based Low-Light Image Enhancement via Neural Implicit Representations. Springer Nature Switzerland. 2024.

[12] Yang, W.; Wang, S.; Fang, Y.; Wang, Y.; Liu, J. From Fidelity to Perceptual Quality: A Semi-Supervised Approach for Low-Light Image Enhancement. In Proceedings of the 2020 IEEE/CVF Conference on Computer Vision and Pattern Recognition (CVPR), Online, 13–19 June 2020; IEEE: New York, NY, USA, 2020.

[13] Juan C. Benito, Daniel Feijoo, Alvaro García, Marcos V. Conde: FLOL: Fast Baselines for Real-World Low-Light Enhancement. CoRR, 2025.

[14] Liu, R.; Ma, L.; Zhang, J.; Fan, X.; Luo, Z. Retinex-inspired Unrolling with Cooperative Prior Architecture Search for Low-light Image Enhancement. In Proceedings of the Computer Vision and Pattern Recognition, Nashville, TN, USA, 19–25 June 2021; IEEE: New York, NY, USA, 2021.

[15] Perez-Zarate, E., Ramos-Soto, O., Liu, C., Oliva, D., & Perez-Cisneros, M. . Alen: a dual-approach for uniform and non-uniform low-light image enhancement. 2024

[16] Li, C.; Guo, C.; Chen, C.L. Learning to Enhance Low-Light Image via Zero-Reference Deep Curve Estimation. IEEE Trans. Softw. Eng. 2021, 44, 555.

[17] Wu, T.; Wang, L.; Zhu, J. Image Edge Detection Based on Sobel with Morphology. In Proceedings of the 2021 IEEE 5th Information Technology, Networking, Electronic and Automation Control Conference (ITNEC), Xi'an, China, 15–17 October 2021; pp. 1216–1220